 CMES, vol.98, no.1, pp.101-127, 2014

Particle-Based Moving Interface Method for The Study of the Interaction Between Soft Colloid Particles and Immersed Fibrous Network

Louis C. Foucard[1], **John Pellegrino**[1] **and Franck J. Vernerey**[1,2]

Abstract: Many colloidal-sized particles encountered in biological and membrane-based separation applications can be characterized as soft vesicles such as cells, yeast, viruses and surfactant micelles. The deformation of these vesicles is expected to critically affect permeation by accommodating pore shapes and sizes or enhancing the adhesion with a pore surface. Numerical and theoretical modelings will be critical to fully understand these processes and thus design novel filtration membranes that target, not only size, but deformability as a selection criterion. The present paper therefore introduces a multiscale strategy that enables the determination of the permeability of a fibrous network with respect to complex fluids loaded with vesicles. The contributions are two-fold. First, we introduce a particle-based moving interface method that can be used to characterized the severe deformation of vesicles interacting with an immersed fibrous network. Second, we present a homogenization strategy that permits the determination of a network permeability, based on the micromechanisms of vesicle deformation and permeation. As a proof of concept, we then investigate the role of vesicle-solvent surface tension on the permeation of both solvent and vesicle through a simple fiber network. We find that vesicles are always retarded relative to the continuum (or solvent) flow, and that the relative selectivity for the continuum versus the vesicle is inversely proportional to the capillary number.

Keywords: Soft vesicles, porous media, Stokes flow, computational homogenization, singular flow around fibers

[1] CU Boulder, Boulder, CO, USA

[2] Corresponding author: Franck J Vernerey, Department of Civil, Environmental and Architectural Engineering, Material science and Engineering, University of Colorado, 1111 Engineering Drive, 428 UCB, ECOT 422 Boulder, CO 80309-0428 USA.

1 Introduction

Filtration membranes are ubiquitous to most biological systems and are at the heart of important applications in bio-medical engineering [Baker (2004); Desai, Hansford, Nashat, Rasi, Tu, Wang, Zhang, and Ferrari (2000)], food industry and both fossil and renewable fuels processes [Cheryan (2005)]. In the majority of these applications, membranes are used to either (a) separate undesired particles from a solution or (b) produce (and fractionate) stable emulsions with specific size controls (such as liposomes) used in medical diagnosis and therapy [Cevc (2004)]. In addition, a novel area of biological medicine is drug delivery using liposomes [Gregoriadis and Florence (1993); Allen and Cullis (2013)]. A liposome is a micron-sized vesicle (bubble) whose interfacial surface is stabilized by lipids. The interior of the liposome can be filled with drugs to be delivered for treatment of various diseases. Filtration of fluids containing liposomes are required at various steps within their manufacture and delivery to patients, in order to provide sterility. These filtration steps can require both allowing liposomes to freely pass through the porous filter, while retaining possible biological contaminants, as well as, retaining and concentrating the liposomes. Despite the very soft nature of these colloidal particles, current membrane designs have consistently relied on the assumptions that they are rigid particles [Faibish, Elimelech, and Cohen (1998); Song (1998); Hoek, Kim, and Elimelech (2002)]. In fact, it has only been in recent years that hindrance factors for transport of non-spheroidal (rod) shaped rigid particles in ideal pores has been theoretically addressed [Baltus, Badireddy, Xu, and Chellam (2009); Dechadilok and Deen (2006)]. This has strongly hindered the performance of current membrane systems. The incorporation of deformation is, however, expected to critically affect the above mechanisms since particles can easily change their shape to accommodate a variety of pore shapes and sizes (Fig. 1). It can also increase the adhesion between a particle and a surface (by effectively increasing the contact surface area) and thus hinder particle entry and permeation.

From a computational modeling viewpoint, studies of the mechanics of soft vesicles and their interactions with an immersed porous network has been hindered by a number of theoretical challenges, which include the coupled fluid-structure interactions, intense particle deformations and perhaps separation, as well as the effect of surface forces that are very significant at micron (and lower) length scales. Furthermore, when fibers are present, the geometry of sharp tips create singular flow fields which have been resolved through the use of refinement methods [Alleborn, Nandakumar, Raszillier, and Durst (1997); Mullin, Seddon, Mantle, and Sederman (2009)]. Such approaches are not only costly but can never truly resolve the steep gradient and hyperbolic pressure field that appears at the fiber tips [Moffatt (1963)]. Regarding modeling immersed vesicles, one of the most acknowledged methods is

the Immersed Boundary Method [Peskin (1972)], which basically relies on three features. First, the fluid flow equations are handled with an classical Eulerian approach. Second, the deformation of the vesicle's boundary (which can be described as a shell, membrane or bi-fluid interface) is done within a Lagrangian frame and third, the fluid-structure interactions are handled via a forcing term that is localized on the membrane domain. Numerous biological problems were approached in this manner, such as red blood cell motion [Eggleton and Popel (1998)], or cell growth and division [Li, Yun, and Kim (2011); Dillon, Owen, and Painter (2008)]. Later improvement of the method includes the Immersed Finite Element Method [Zhang, Gerstenberger, and Wang (2002)], where the Lagrangian solid mesh evolves on top of a background Eulerian mesh that covers the entire computational domain. This simplifies greatly the mesh generation. Another computational method for the treatment of fluid-solid interactions is the Immersed Particle Method, where both the fluid and the structure are described using Lagrangian mesh free particles [Rabczuk, Gracie, Hsong, and Belytschko (2000)]. However, due to the lagrangian treatment of interfaces, these methods becomes cumbersome when extreme deformations and subsequently severe distortions of the finite element mesh or the particle distribution are observed. The use of mesh regularization techniques [Ma and Klug (2008)] may provide a solution but they remain computationally expensive. When studying vesicle permeation through porous media, a second challenge is to link macroscopic models, traditionally casted in terms of Darcy's law Chen, Huan, and

derivative $\mathbf{v}(\mathbf{x};t) = D\mathbf{x}/Dt$, where $\mathbf{x} = fx\ \ yg$ is the current position of the fluid particle at time t. Under these conditions, the governing equations and boundary conditions for the Stokes flow are written:

$$\tilde{N}\ s = \mathbf{0} \qquad 8\mathbf{x}\ 2\ W/G \tag{1}$$

$$\tilde{N}\ \mathbf{v} = 0 \qquad 8\mathbf{x}\ 2\ W/G \tag{2}$$

where s is the Cauchy stress tensor in the fluid and the second equation imposes the condition of incompressibility. These equations are combined with the moving interface problem:

$$[s\ \ \mathbf{n}] = \mathbf{f}_I + \mathbf{f}_{F=I} \qquad 8\mathbf{x}\ 2\ G_I \tag{3}$$

$$D\mathbf{X}_I(t)/Dt = \mathbf{v}(\mathbf{x}(\mathbf{X}_I;t);t) \qquad 8\mathbf{x}\ 2\ G_I \tag{4}$$

Here $\mathbf{X}_I$

on the order of the particle size and finally, microscopic fields vary on the order of the fiber diameter size. This creates a significant issue to later derive an accurate numerical solution at a reasonable computational cost. Inspired by asymptotic methods [Hawa and Rusak (2002); Moës, Dolbow, and Belytschko (1999)], we here propose to address the problem as follows; First, we derive a solution for the fluid flow around the tip of a fiber and subjected to the far-fields boundary conditions. Then, we enrich our macroscopic solution with this solution in the regions of interests, which result in introducing a limited number of "microscopic" degrees of freedom. Finally, we compute a solution that ensures that both microscopic and mesoscopic are consistent within the entire computational domain.

To simplify our analysis, let us first assume that the width of our fibers is infinitesimally small compared to other dimensions of the problem. In this case, the flow field near the tip of fibers admits a singular solution that was derived by Moffat in [Moffatt (1963)]. Adopting a polar coordinate system $(r;q)$ centred on the fiber tip, where $r = \sqrt{x'^2 + y'^2}$, $q = \arctan(y'/x')$ and the axis x' and y' are aligned with the fiber (Fig. 1). The streamline function $y(r;q)$ solution to the Stokes equation $\tilde{N}y = 0$ in the region $0 < r$ H can be written in the following separated form:

$$y(r;q) = r^a f_a(q) \tag{10}$$

where a is an unknown complex exponent that determines the structure of the flow, and is to be found as part of the solution. Following [Moffatt (1963)], the function $f_a(q)$ is written:

$$f_a(q) = A\cos(aq) + B\sin(aq) + C\cos((a \quad 2)q) + D\sin((a \quad 2)q) \tag{11}$$

where $A;B;C$ and D are arbitrary complex constants. In the cases where $a = 0;1$ or 2, the above equation degenerates into other forms that are not relevant to the problem studied here, and we will henceforth only consider values of a such that $a \neq 0;1;2$. The axial and radial velocities of the flow are deduced from the stream function $y(r;q)$ as follows:

$$v_r = \frac{1}{r}\frac{\P y}{\P q} \quad \text{and} \quad v_q = \quad \frac{\P y}{\P r}; \tag{12}$$

and are subjected to the following no-slip/no-penetration boundary conditions at the wall:

$$v_r(r;q = a) = 0; \quad v_q(r;q = a) = 0 \tag{13}$$

Enforcing these boundary conditions on (12) and (11) yields the constant $A;B;C$ and D [Moffatt (1963)] are = [illegible] cos[illegible] are 4

as well as the exponent a, found to be $a = 3=2$ in the particular case of infinitesimally thin fibers [Moffatt (1963)]. The pressure can then be calculated by solving the momentum equation

$$\tilde{N}p = m\tilde{N}^2\mathbf{v} \tag{15}$$

where $\mathbf{v} = v_r\mathbf{e}_r + v_q\mathbf{e}_q$ is computed using equations (10) and (12).

3 Numerical approach: the Particle Enriched Moving Interface Method

The idea of the Extended Finite Element Method is to enrich a finite element space with additional functions. Our numerical technique takes the same approach: the Stokes flow is solved using the traditional C_0 conforming finite elements (in our cases 4 node bilinear elements for the pressure and 9 node quadratic elements for the velocity) space, and we enrich this space with additional degrees of freedom that allow the pressure jump across the interface (the velocity stays continuous) and singular pressure and velocity fields around the corner tip. To enrich the standard finite element space, we make use of the linearity of the Stokes flow and simply sum the enrichments for the pressure jump and the asymptotic solution around the corner tip. The velocity and pressure fields in this enriched space are therefore interpolated as follows:

$$\begin{aligned} p(\mathbf{x}) &= \sum_i N_i(\mathbf{x})p_i + \sum_j N_j(\mathbf{x})(H(f_F(\mathbf{x})) \quad H_j)\check{p}_j \\ &+ \sum_k \sum_l N_k(G^l(r(\mathbf{x}); q(\mathbf{x})) \quad G_k)\hat{p}_k \\ &+ \sum_j N_j(\mathbf{x})(H(f_l \end{aligned}$$

Table 1: Corner tip asymptotic functions

G	$r^{a\ \ 2}\sin(aq); r^{a\ \ 2}\sin((a_1\ \ 2)q); r^{a\ \ 2}\cos(aq); r^{a\ \ 2}\cos((a\ \ 2)q)$
F	$r^{a\ \ 1}\sin((a\ \ 2)q)\sin q; r^{a\ \ 1}\cos((a_1$ $\sin((a\ \ 2$

$l \in L$ and $l_p \in L_p$ such that for all $\mathbf{w_v} \in V$, $w_p \in P$, $\mathbf{w}_l \in L$ and $w_{l_p} \in L_p$

$$
\begin{aligned}
&(\tilde{N}\mathbf{w_v}; m\tilde{N}\mathbf{v})_W \quad (\tilde{N}\mathbf{w_v}; p\mathbf{I})_W + (\mathbf{w_v}; r\,\mathbf{f})_W + (\mathbf{w_v}; l)_G + \mathbf{w_v}; \mathbf{f}_l + \mathbf{f}_{R=l})_G = 0 \\
&(w_p; \tilde{N}\ \mathbf{v})_W + (w_p; l_p)_G = 0 \\
&(w_{l_p}; [p])_G + (w_{l_p}; (\mathbf{f}_l + \mathbf{f}_{R=l})\ \mathbf{n})_G = 0 \\
&(\mathbf{w}_l; \mathbf{v})_G = 0
\end{aligned}
\tag{18}
$$

where the notation $(\ ;\ )_W$ indicates the L^2 inner product with respect to the domain W. The Lagrange multipliers l and l_p enforce the no-slip/no-penetration boundary conditions (6) and the pressure jump conditions on the implicitly defined corner walls. The test functions $\mathbf{w}_l$ and w_{l_p} are associated with the Lagrange multipliers and V, P, L and L_p are admissible spaces for the velocity, pressure and Lagrange multipliers.

3.2 Discretized form

The weak form (18) is then discretized in space by using the XFEM approximation, and after simplifications yields the following linear system:

$$\mathbf{K}^t\mathbf{d}^t = \mathbf{f}^t \tag{19}$$

where $\mathbf{K}^t$ is the consistent tangent matrix, $\mathbf{d}^t = f\mathbf{v}\ \ p\ \ l_p\ \ l g$ the global vector of unknowns and $\mathbf{f}^t$ the global force vector at time t. The element contribution to $\mathbf{K}^t$ and $\mathbf{f}^t$ are as follows:

$$
\mathbf{k}^e = \begin{bmatrix} \mathbf{k}^e_{\mathbf{vv}} & \mathbf{k}^e_{\mathbf{v}p} & 0 & \mathbf{k}^e_{\mathbf{v}l} \\ \mathbf{k}^e_{p\mathbf{v}} & 0 & \mathbf{k}^e_{pl_p} & 0 \\ 0 & \mathbf{k}^e_{l_pp} & 0 & 0 \\ \mathbf{k}^e_{l\mathbf{v}} & 0 & 0 & 0 \end{bmatrix}; \quad \mathbf{f}^e = \begin{Bmatrix} \mathbf{f}^e_{\mathbf{v}} & 0 & \mathbf{f}^e_{l_p} & 0 \end{Bmatrix}^T; \tag{20}
$$

The form of the components in the $\mathbf{k^e}$ matrix and and the $\mathbf{f}^e$ are given in appendix A. The finite element equation (19) can be solved with a linear solver to yield an expression for the fluid (and interface) velocity $\mathbf{v}$ at time t. Given the interface velocity $\mathbf{v}$, the position $\mathbf{X}_l$ of the vesicle interface G_l is then updated to compute $\mathbf{K}^{t+dt}$ and $\mathbf{f}^{t+dt}$ for the next time step, with dt the time step increment. Once the vesicle has left the computational domain, or once $jj\mathbf{d}^{t+dt} \quad \mathbf{d}^t jj < TOL$, the algorithm has converged and the interface is in equilibrium with the surrounding fluid. The next step involves the transport of the interface using a mesh-based particle method, as discussed next.

3.3 Grid based particle method for interface evolution

To track the deformation of the interface G_I, we choose here to use a grid-based particle method similar to what was introduced in [Leung, Lowengrub, and Zhao (2011)]. This method indeed possesses the double advantage of tracking the interface explicitly with particles while using the underlying fixed finite element mesh to ensure a fairly uniform repartition of the particles on the interface. Here we summarize the grid based particle method and discuss the update of the interface position and deformations measures. The particles, whose position vector is denoted by **y**, are chosen as the normal projection of the underlying mesh nodes, with position vector **p**, on G (Fig. 3a.). Initially, the interface is described implicitly as the zero level-set of a signed distance function $f_I(\mathbf{p};t=0)$. The initial coordinates of particles **y** can then found as follows:

$$\mathbf{y} \quad = \quad \mathbf{p} \quad f_I(\mathbf{p};0)\tilde{N} f_I(\mathbf{p};0) \tag{21}$$

To limit the number of particles, we define a so-called computational tube such that only nodes **p** whose distance to G_I is smaller than a cut-off value l_{tube} are accounted for. It is important to note here that there is a one to one correspondence between each particle **y** and node **p**. This ensure a quasi-uniform repartition of particles along the interface throughout its evolution. Between two subsequent time steps, the particles are moved according to the normal component of the interface velocity $\mathbf{v}^{?}(x;t)$ as follows:

$$\mathbf{y}^{t+dt} \quad = \quad \mathbf{y}^t + \mathbf{v}^{?}(\mathbf{y}^t;t)dt + W \;\; \mathbf{v}^{?}(\mathbf{y}^t;t)\frac{dt^2}{2} \tag{22}$$

where W is the matricial form of the angular velocity of the interface normal [Jason and Kumar (2012)]:

$$w \;=\; \quad v^{?}_{;x_1} \;\; [0\;0\;1]^T \quad \text{and} \quad W_{ik} \;=\; e_{ijk}w_j \tag{23}$$

with e_{ijk} the permutation tensor and x_1 the local coordinate running along the interface (Fig. 3b.). After the motion of the interface, the particles **y** may not be the closest point on G_I to their associated nodes **p**. Moreover, the motion of the particles may cause their distribution onc with particles TJ/F interface the respond ed

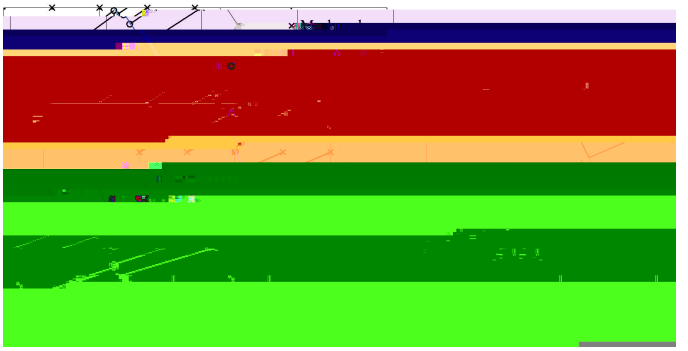

Figure 3: *(a) particles and associated nodes in the computational tube. (b) Local polynomial approximation of the surface (and of any Lagrangian field). The polynomial* $x^3(x^1;x^2)$ *that approximates the interface is constructed via least square fitting using neighbouring particles in the local referential* $f\mathbf{a}_0;\bar{\mathbf{n}}_0g$ *centered on particle* $\mathbf{y}_0$.

case, is as follows: for each node $\mathbf{p}$ inside the computational tube, the closest m particles $\mathbf{y}_0:::\mathbf{y}_m$ are collected, carrying with them the tangent $\mathbf{a}_0^t:::\mathbf{a}_m^t$ and normal $\bar{\mathbf{n}}_0^t:::\bar{\mathbf{n}}_m^t$ to the interface before motion. Denoting $\mathbf{y}_0$ as the particle closest to $\mathbf{p}$, a polynomial of degree $n < m$ is fitted to the particles $\mathbf{y}_0:::\mathbf{y}_m$ in the local coordinate system $f\mathbf{s}_0^t;\bar{\mathbf{n}}_0^tg$ centered on $\mathbf{y}_0$ (Fig.3b). The location $\tilde{\mathbf{y}}_i$ of particle i in this local coordinate system is given by:

$$\tilde{\mathbf{y}}_i = \begin{matrix} x_i^1 \\ x_i^2 \end{matrix} = \mathbf{R}^t \ (\mathbf{y}_i \quad \mathbf{y}_0) \ \text{with} \ \mathbf{R}^t = \begin{matrix} (\mathbf{a}_0^t)^T \\ (\bar{\mathbf{n}}_0^t)^T \end{matrix} : \tag{24}$$

Taking the example of a quadratic polynomial ($n = 2$), the interface around particle $\mathbf{y}_0$ is represented in the local referential as the graph function $x^2(x^1) = c_0 + c_1x^1 + c_2(x^1)^2$, where the coefficients $c_0;c_1$ and c_2 are found by minimizing the L^2 difference between the $x^2(x_i^1)$ and the x_i^2. The coordinates $x^1;x^2(x^1)$ defines a local parameterization $\mathbf{r}^l(x^1)$

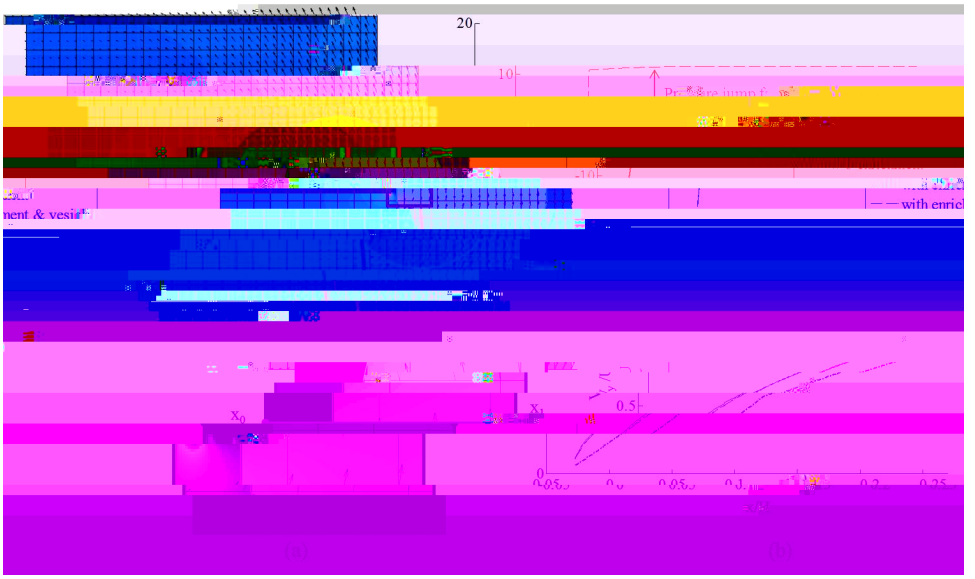

Figure 4: *Error E_v made in computing the flow velocity around the corner tip in mode I and II, for different corner angle α. The error can be lessened by more then a factor of 10 using corner tip enrichment.*

domain. The error made in computing the velocity of the flow near a corner is calculated as follows:

$$E_v = \int_{x_0}^{x_1} \| \mathbf{v}_{num} - \mathbf{v} \| \, dx$$

as a close up of the singular pressure field around the fiber tip and the pressure jump across the vesicle interface. Fig.4b. shows the velocity and the pressure field in the neighbourhood of the fiber tip, along the line from point $\mathbf{x}_0$ to $\mathbf{x}_1$. We observe in table 2 that without enrichment, the errors E_v and E_p are fairly high, at 18.2% and 22.1% respectively. However, the incorporation of the tip enrichment developed above reduces the errors down to 0.7% and 3.1% respectively. The presence of a circular vesicle in the vicinity of the fiber tip does not significantly affect the accuracy of the scheme, and we can note the appearance of a pressure jump across the vesicle interface from its surface tension, as expected. The source of the remaining error stems from the weak enforcement of the no-slip/no-penetration condition on the corner wall. Future studies will investigate reducing the error by using quadratic instead of linear shape function for the interpolation of Lagrange multipliers. Overall, the numerical technique presented here is shown to significantly increase the accuracy of the simulation of a flow near a sharp corner using the extended finite element method, at a much lesser computational cost than classical methods since no mesh refinement is needed.

4 Numerical approach to predict the permeation of a soft colloids though a fibrous network

In this section, we present a generalized homogenization scheme to determine how different phases of a fluid (such as solvent or various vesicles present in the solvent) can permeate through a fibrous filtration membrane. For this, we first present a general homogenization scheme based on the Hill-Mendel conditions that then served as a basis to express macroscopic permeabilities in terms of flux and pressure on the boundary of a volume element. We then apply these concepts to the specific problem of soft vesicles travelling through a small fibrous network and pay particular attention to the role of surface tension at the vesicle-solvent interface.

4.1 General homogenization scheme to compute macroscopic permeabilities

From a macroscopic viewpoint, the phenomenon of fluid flow through porous media has traditionally been described by Darcy's law relating volumic flux to pressure gradient throughout a porous network. The relationship between the flux $\mathbf{Q}_a$ of fluid a and the macroscopic pressure gradient $\bar{\tilde{\nabla}}\bar{p}$ is established via the definition of so-called macroscopic permeability tensor k_a in the form

$$\mathbf{Q}_a = \frac{k_a}{m_a}\bar{\tilde{\nabla}}\bar{p} \tag{34}$$

where m_a is the fluid viscosity. We note that for isotropic porous network such as those studied in this paper, the permeability can be expressed in terms of a single

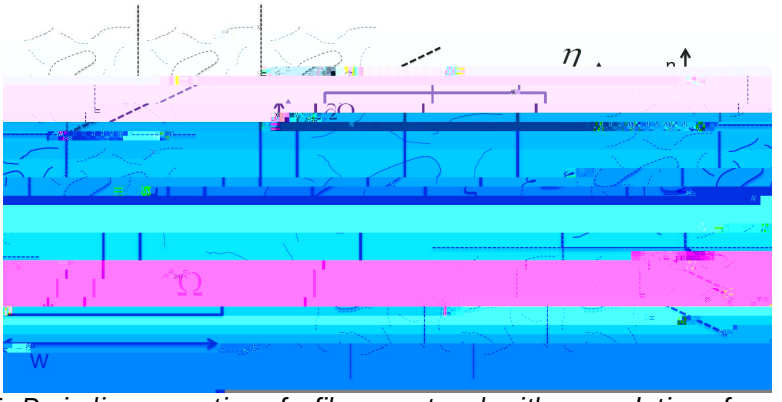

Figure 5: *Periodic assumption of a fibrous network with a population of permeating particles. A unit periodic cell is identified and analysized to extract the macroscopic properties of the network.*

scalar quantity k_a such that $k_a = k_a \mathbf{I}$ with $\mathbf{I}$ representing the second order identity tensor.

It is clear here that the quantity k_a represents the ease by which a fluid permeated through the network. Theoretically, it may therefore be determined through a thorough study of the micromechanisms of vesicle flow and deformation and a consistent averaging operation to bridge micro to macroscale. We propose here to use classical homogenization theory where we assume that at the mesoscale, a membrane is made of a periodic array of unit cells comprised of a pseudo-random fiber distribution. For the sake of simplicity, we also assume that a number of vesicles can be found within each of these cells and that they all have the same position relative the their corresponding unit cells (Fig. 5). For each elementary volume (of dimension, W H

with **n** the unit vector normal to the boundary G and V_0 the volume of the domain. Note that we used the divergence theorem to obtain the last equality. The above relation is particularly useful as it enables to characterise the macroscopic pressure

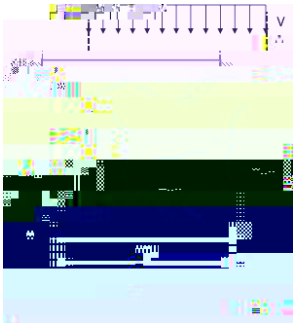

Figure 6: *Schematic of the geometry, dimensions and boundary conditions for assessing the permeation of a soft colloid particle through a fibrous network.*

conditions are given in terms of the macroscopic solvent flow $q_s = V$ and a no-flux boundary condition on the left and right boundaries of the domain. The relevant quantities to compute are therefore (a) the overall vertical solvent flux Q_y^s, (b) the overall vertical vesicle flux Q_v^s and the vertical macroscopic pressure gradient $\tilde{\tilde{N}}_y \bar{p}$. For each simulation, the elementary time Dt is computed as the time required for a vesicle to travel the entire (vertical) length of the domain.

Flux. For this particular problem, the homogenization relation (39) becomes, for the solvent:

$$Q_y^s = \frac{1}{WH\mathrm{D}t} \int_{\mathrm{D}t} \int_{x=-W/2}^{W/2} (HV dx)\, dt = V \tag{40}$$

where the final equality was obtained by realizing that the volumic flux of the fluid across the boundary is constant in time. The volumic flux of vesicle can similary be computed by:

$$Q_y^v = \frac{1}{WH\mathrm{D}t} \int_{\mathrm{D}t} \int_{x=-W/2}^{W/2} (Hv_v dx)\, dt = f^v \frac{H}{\mathrm{D}t} \tag{41}$$

where we used the fact that for incompressible fluids, the cumulative volumic flux entering the domain during a time interval Dt is equal to the volume W^v in the vesicle. In other words, we have:

$$\mathrm{W}^v = \int_{\mathrm{D}t} \int_{x=-W/2}^{W/2} (v_v dx)\, dt \tag{42}$$

This relation, together with the expression of the volume fraction of a vesicle $f^v = \mathrm{W}^v/(WH)$ yields the second equality in (41). This result indicates that the volumic

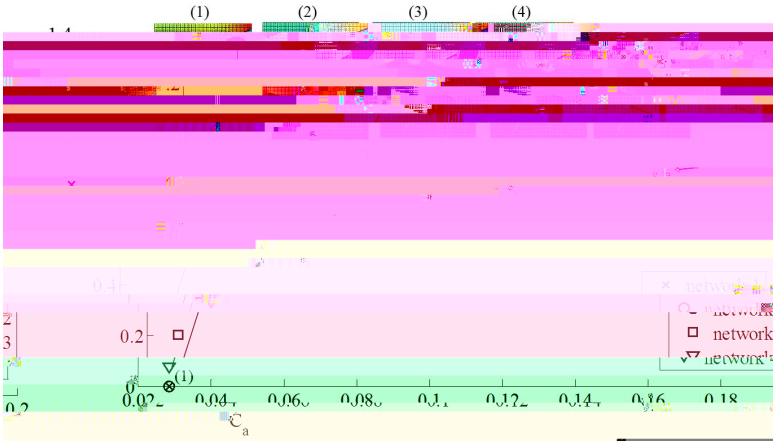

Figure 8: *Vesicle permeability as a function of the capillary number C_a*

and

$$\mathbf{f}_{\mathbf{v}}^{e} = \int_{\Omega^e} \mathbf{N}^T \rho \mathbf{f}\, d\Omega + \int_{\Gamma^e} \mathbf{N}^T (\mathbf{f}_I + \mathbf{f}_{R=I})\, d\Gamma; \tag{47}$$

$$\mathbf{f}_{I_p}^{e} = \int_{\Gamma^e} \bar{\mathbf{N}}^T \mathbf{n} (\mathbf{f}_I + \mathbf{f}_{R=I})\, d\Gamma; \tag{48}$$

The shape function matrices $\mathbf{N}$, $\hat{\mathbf{N}}$, $\check{\mathbf{N}}$ and $\mathbf{B}$ take the following form:

$$\mathbf{N} = \left[\mathbf{N}^1;\ldots;\mathbf{N}^9;\tilde{\mathbf{N}}^1;\ldots;\tilde{\mathbf{N}}^9\right] \tag{49a}$$

$$\hat{\mathbf{N}} = \left[\hat{N}^1;\ldots;\hat{N}^4;\check{N}^1;\ldots;\check{N}^4;\tilde{\hat{N}}^1;\ldots;\tilde{\hat{N}}^4\right] \tag{49b}$$

$$\bar{\mathbf{N}} = \left[\bar{N}^1\ \bar{N}^2\right] \tag{49c}$$

$$\mathbf{B} = \left[\mathbf{B}^1;\ldots;\mathbf{B}^9;\tilde{\mathbf{B}}^1;\ldots;\tilde{\mathbf{B}}^9\right] \tag{49d}$$

with

$$\mathbf{N}^i = \begin{bmatrix} N^i & 0 \\ 0 & N^i \end{bmatrix};\ \tilde{\mathbf{N}}^i = \begin{bmatrix} (F-F^1)\begin{bmatrix} N^i & 0 \\ 0 & N^i \end{bmatrix};\ldots;(F-F^8)\begin{bmatrix} N^i & 0 \\ 0 & N^i \end{bmatrix} \end{bmatrix} \tag{50a}$$

$$\check{N}^i = (H-H^i)\hat{N}^i;\ \tilde{\hat{N}}^i = \left[(G-G^1)\hat{N}^i;\ldots;(G-G^4)\hat{N}^i\right] \tag{50b}$$

$$\mathbf{B}^i = \begin{bmatrix} N^i_{;1} & 0 \\ 0 & N^i_{;2} \\ N^i_{;2} & 0 \\ 0 & N^i_{;1} \end{bmatrix} \tag{50c}$$

$$\tilde{\mathbf{B}}^i = \left[\begin{bmatrix} (F-F^1)N^i)_{;1} & 0 \\ 0 & (F-F^1)N^i)_{;2} \\ (F-F^1)N^i)_{;2} & 0 \\ 0 & (F-F^1)N^i)_{;1} \end{bmatrix};\ldots;\begin{bmatrix} (F-F^8)N^i)_{;1} & 0 \\ 0 & (F-F^8)N^i)_{;2} \\ (F-F^8)N^i)_{;2} & 0 \\ 0 & (F-F^8)N^i)_{;1} \end{bmatrix}\right]. \tag{50d}$$

where F^i and G^i are the asymptotic functions used to enriched the standard finite element space around the corner tips introduced earlier.

References

Alleborn, N.; Nandakumar, K.; Raszillier, H.; Durst, F. (1997): Further contributions on the two-dimensional flow in a sudden expansion. *Journal of Fluid Mechanics*, vol. 330, pp. 169–188.

Allen, T. M.; Cullis, P. R. (2013): Liposomal drug delivery systems: from concept to clinical applications. *Advanced drug delivery reviews*, vol. 65, no. 1, pp. 36–48.

Baker, R. (2004): *Membrane technology and applications*. 2nd edition.

Baltus, R. E.; Badireddy, A. R.; Xu, W.; Chellam, S. (2009): Analysis of Configurational Effects on Hindered Convection of Nonspherical Bacteria and Viruses across Microfiltration Membranes. *Industrial & Engineering Chemistry Research*, vol. 48, no. 5, pp. 2404–2413.

Cevc, G. (2004): Lipid vesicles and other colloids as drug carriers on the skin. *Advanced drug delivery reviews*, vol. 56, no. 5, pp. 675–711.

Chen, Z.; Huan, G.; Ma, Y. (2006): *Computational Methods for Multiphase Flows in Porous Media*. SIAM.

Cheryan, M. (2005): Membrane technology in the vegetable oil industry. *Membrane Technology*, vol. 2005, no. 2, pp. 5–7.

De Gennes, P. G.; Brochard-Wyart, F.; Quere, D. (2004): *Capillarity and Wetting Phenomena*. Springer.

Dechadilok, P.; Deen, W. M. (2006): Hindrance Factors for Diffusion and Convection in Pores. *Industrial & Engineering Chemistry Research*, vol. 45, no. 21, pp. 6953–6959.

Desai, T. A.; Hansford, D. J.; Nashat, A. H.; Rasi, G.; Tu, J.; Wang, Y.; Zhang, M.; Ferrari, M. (2000): Nanopore Technology for Biomedical Applications. pp. 11–40.

Dillon, R.; Owen, M.; Painter, K. (2008): A single-cell-based model of multicellular growth using the immersed boundary method. *Contemporary Mathematics*, vol. 466, no. 1, pp. 1–15.

Eggleton, C. D.; Popel, A. S. (1998): Large deformation of red blood cell ghosts in a simple shear flow. *Physics of Fluids*, vol. 10, no. 8, pp. 1834.

Faibish, R.; Elimelech, M.; Cohen, Y. (1998): Effect of Interparticle Electrostatic Double Layer Interactions on Permeate Flux Decline in Crossflow Membrane Filtration of Colloidal Suspensions: An Experimental Investigation. *Journal of colloid and interface science*, vol. 204, no. 1, pp. 77–86.

Foucard, L.; Vernerey, F. J. (2012): A thermodynamical model for stress-fiber organization in contractile cells. *Applied Physics Letters*, vol. 100, no. 1, pp. 13702–137024.

Foucard, L. C.; Vernerey, F. J. (2014): An X-FEM based numerical-asymptotic expansion for simulating a Stokes flow near a sharp corner. *IJNME (under review)*.

Foucard, L. C.; Vernerey, F. J. (2014): Particle-based Moving Interface Method for the study of immersed soft vesicles. *IJNME (under review)*, pp. 1–31.

Gregoriadis, G.; Florence, A. (1993): Liposomes in drug delivery. Clinical, diagnostic and ophthalmic potential. *Drugs*, vol. 45, no. 1, pp. 15–28.

Hawa, T.; Rusak, Z. (2002): Numerical-Asymptotic Expansion Matching for Computing a Viscous Flow Around a Sharp Expansion Corner. pp. 265–281.

Hoek, E. M. V.; Kim, A. S.; Elimelech, M. (2002): Influence of Crossflow Membrane Filter Geometry and Shear Rate on Colloidal Fouling in Reverse Osmosis and Nanofiltration Separations. *Environmental Engineering Science*, vol. 19, no. 6, pp. 357–372.

Jason, H.; Kumar, T. (2012): *Advances in Computational Dynamics of Particles, Materials and Structures*. John Wiley & Sons, Ltd.

Leung, S.; Lowengrub, J.; Zhao, H. (2011): A Grid Based Particle Method for Solving Partial Differential Equations on Evolving Surfaces and Modeling High Order Geometrical Motion. *J25.10tFnal of Computational Physics*

Song, L. (1998): Flux decline in crossflow microfiltration and ultrafiltration: mechanisms and modeling of membrane fouling. *Journal of Membrane Science*, vol. 139, no. 2, pp. 183–200.

Vernerey, F.; Liu, W. K.; Moran, B. (2007): Multi-scale micromorphic theory for hierarchical materials. *Journal of the Mechanics and Physics of Solids*, vol. 55, no. 12, pp. 2603–2651.

Vernerey, F. J. (2011): A theoretical treatment on the mechanics of interfaces in deformable porous media. *International Journal of Solids and Structures*, vol. 48, no. 22-23, pp. 3129–3141.

Vernerey, F. J. (2012): The Effective Permeability of Cracks and Interfaces in Porous Media. *Transport in Porous Media*, vol. 93, no. 3, pp. 815–829.

Vernerey, F. J.; Farsad, M. (2011): A constrained mixture approach to mechano-sensing and force generation in contractile cells. *Journal of the mechanical behavior of biomedical materials*, vol. 4, no. 8, pp. 1683–99.

Vernerey, F. J.; Foucard, L.; Farsad, M. (2011): Bridging the Scales to Explore Cellular Adaptation and Remodeling. *BioNanoScience*, vol. 1, no. 3, pp. 110–115.

Zhang, L.; Gerstenberger, A.; Wang, X. (2002): Immersed Finite Element Method. *Computer Methods in Applied Mechanics and Engineering*, , no. September 2003, pp. 1–25.